INSTITUT DE FRANCE
Académie des sciences

Comptes Rendus

Géoscience

Sciences de la Planète

Alessandro Aiuppa and Yves Moussallam

Hydrogen and hydrogen sulphide in volcanic gases: abundance, processes, and atmospheric fluxes

Published online: 26 September 2023

https://doi.org/10.5802/crgeos.235

Part of Special Issue: Magma degassing and its impact on the Earth's atmosphere: from magma oceans to lava lakes

Guest editors: Manuel Moreira (Institut des Sciences de la Terre d'Orléans Université d'Orléans-CNRS-BRGM 1a rue de la Férollerie 45071 Orléans France), Bruno Scaillet (Institut des Sciences de la Terre d'Orléans Université d'Orléans-CNRS-BRGM 1a rue de la Férollerie 45071 Orléans France) and Clive Oppenheimer (Department of Geography, University of Cambridge, Downing Place, Cambridge CB2 3EN, UK)

Les Comptes Rendus. Géoscience — Sciences de la Planète *sont membres du Centre Mersenne pour l'édition scientifique ouverte*
www.centre-mersenne.org
e-ISSN : 1778-7025

Comptes Rendus
Géoscience — Sciences de la Planète
Published online: 26 September 2023
https://doi.org/10.5802/crgeos.235

Magma degassing and its impact on the Earth's atmosphere: from magma oceans to lava lakes

Hydrogen and hydrogen sulphide in volcanic gases: abundance, processes, and atmospheric fluxes

Alessandro Aiuppa *, [a] **and Yves Moussallam** [b]

[a] Dipartimento di Scienze della Terra e del Mare, Università di Palermo, Palermo, Italy

[b] Lamont-Doherty Earth Observatory, Columbia University, New York, USA

E-mails: alessandro.aiuppa@unipa.it (A. Aiuppa),
yves.moussallam@ldeo.columbia.edu (Y. Moussallam)

Abstract. Hydrogen (H_2) and hydrogen sulphide (H_2S) are typically present at only minor to trace levels in volcanic gas emissions, and yet they occupy a key role in volcanic degassing research in view of the control they exert on volcanic gas reducing capacity (e.g., their ability to remove atmospheric O_2). In combination with other major compounds, H_2 and H_2S are also key to extracting information on source magma conditions (temperature and redox) from observed magmatic gas compositions. Here, we use a catalogue, compiled by extracting from the geological literature a selection of representative analyses of magmatic to mixed (magmatic–hydrothermal) gases, to review the processes that control H_2 and H_2S abundance in volcanic gases. We show that H_2 concentrations and H_2/H_2O ratios in volcanic gases both exhibit strong positive temperature dependences, while H_2S concentrations and H_2S/SO_2 ratios are temperature insensitive overall. The high H_2 concentrations (and low H_2S/SO_2 compositions, of ~0.1 on average) in high-temperature (>1000 °C) magmatic gases are overall consistent with those predicted thermodynamically assuming external redox buffering operated by the coexisting silicate melt, at oxygen fugacities ranging from ΔFMQ −1 to 0 (non-arc volcanoes) to ΔFMQ 0 to +2 (arc volcanoes) (where ΔFMQ is oxygen fugacity expresses as a log unit difference relative to the Fayalite–Magnetite–Quartz oxygen fugacity buffer). Lower temperature (<1000 °C) volcanic gases exhibit more oxidizing redox conditions (typically above the Nickel–Nickel Oxide buffer) that are caused by a combination of (i) gas re-equilibration during closed-system (gas-phase only) adiabatic cooling in a gas-buffered system, and (ii) heterogenous (gas–mineral) reactions. We show, in particular, that gas-phase equilibrium in the H_2–H_2S–H_2O–SO_2 system is overall maintained upon cooling down to ~600 °C, while quenching of higher temperature equilibria (at which Apparent Equilibrium Temperatures, AETs, largely exceed measured discharge temperatures) is more frequently observed for higher extents of cooling (e.g., at $T < 600$ °C). In such lower temperature volcanic environments, gas–mineral reactions also become increasingly important, scavenging magmatic SO_2 and converting it into H_2S and hydrothermal minerals (sulphates and sulphides). These heterogeneous reactions, when occurring, can also control the temperature dependence of the volcanic gas H_2/H_2O ratios. Finally, by using our volcanic gas dataset in tandem with recently published global volcanic SO_2 and CO_2 budgets,

* Corresponding author.

we provide refined estimates for total H_2S (median, 1.4 Tg/yr; range, 0.9–8.8 Tg/yr) and H_2 (median, 0.23 Tg/yr; range, 0.06–1 Tg/yr) fluxes from global subaerial volcanism.

Keywords. Hydrogen, Hydrogen sulphide, Volcanic gases, Volcanic gas redox, Atmospheric fluxes.
Published online: 26 September 2023

1. Introduction

At the relatively oxidised redox conditions of present day Earth's upper mantle [e.g., Frost and McCammon, 2008, Stagno et al., 2013], the magmatic gas phase delivered to the atmosphere by shallow degassing, mantle-sourced magmas is dominated by oxidised molecular combinations of the elements H, C, O and S, e.g., by water (H_2O) carbon dioxide (CO_2) and sulphur dioxide (SO_2) [e.g., Gerlach and Nordlie, 1975, Symonds et al., 1994, Giggenbach, 1996, Fischer and Chiodini, 2015]. However, volcanoes also release a variety of reduced gas species such as molecular hydrogen (H_2) and hydrogen sulphide (H_2S) that, while making up a relatively small fraction of the magmatic gas phase, convey information on a variety of magma-related topics and processes [e.g., Moussallam et al., 2019b, Moretti and Stefánsson, 2020]. For example, studying the release of H_2, H_2S and other reduced gas species (e.g., carbon monoxide, CO) from modern subaerial volcanoes helps setting constraints on the composition of the early atmosphere in the Hadean and the Archean [e.g., Kasting et al., 1993, Gaillard et al., 2015], and to predict the temporal evolution and progressive oxygenation of the atmosphere through geological time [e.g., Holland, 2002, Gaillard et al., 2011, Gaillard and Scaillet, 2014]. Measuring H_2 and H_2S in combination with their oxidised complements H_2O and SO_2 brings information on the redox conditions of magmatic gases [e.g., Ellis, 1957, Matsuo, 1962, Gerlach, 1979, 1982, 1993a,b, Shinohara et al., 1993, Ohba et al., 1994, Symonds et al., 1994, Burgisser and Scaillet, 2007, Oppenheimer et al., 2018, Moussallam et al., 2019b, 2022], and can potentially allow constraining oxygen fugacity of the source magmas. H_2 and H_2S in volcanic gases can also effectively contribute to volcano monitoring [e.g., Kern et al., 2022]. For example, H_2S is a key component of the hydrothermal gases released by quiescent, closed-conduit volcanoes [e.g., Giggenbach, 1980], so that monitoring the H_2S/SO_2 ratio is critical to detecting (and interpreting) the magmatic unrest that proceeds volcanic activity resumption [e.g., Surono et al., 2012, Moussallam et al., 2014b, Stix and de Moor, 2018, de Moor et al., 2019], and to distinguish internally triggered (volcano-related) gas changes from those caused by external factors (e.g., rainfall and/or water level changes) [Moretti et al., 2020, Moune et al., 2022]. A model for estimating magmatic variables (temperature and redox) from the combined analysis of H_2S/SO_2 and H_2/H_2O ratios in volcanic plumes has recently been proposed that promises to become a useful volcano monitoring tool [Moussallam et al., 2022]. Volcano-released H_2 and H_2S are dispersed into the atmosphere through volcanic plumes, where concentrations at ppm levels are typically observed, well in excess of those typical of ambient air [of respectively ~0.5 ppm and ~0.1–0.3 ppb; Seinfeld and Pandis, 2016]. Such in-plume H_2 and H_2S measurements [e.g., Aiuppa et al., 2005, 2011] are useful to interpreting reaction mechanisms and rates, and ultimately lifetime of reduced compounds, during oxidative atmospheric processing, both near-vent [e.g., Martin et al., 2006, Roberts et al., 2019] and in the colder, more distal plumes [e.g., Aiuppa et al., 2007]. Although observations indicate H_2 and H_2S are conserved during atmospheric dispersion over short timescales (seconds to days) [e.g., Aiuppa et al., 2007, 2011], these species are ultimately oxidised directly (by molecular oxygen, O_2) or indirectly (via O_2-derived radicals, such as hydroxyl radicals) during longer atmospheric transit, thus controlling the reducing power (e.g., the ability to act as atmospheric O_2 sinks) of volcanic gases [e.g., Stolper et al., 2021].

Despite their importance in such a variety of subjects, and notwithstanding that excellent reviews are available on magmatic and hydrothermal gases in general [e.g., Giggenbach, 1980, 1996, Symonds et al., 1994, Chiodini and Marini, 1998, Fischer and Chiodini, 2015, Henley and Fischer, 2021], no specific study has so far been devoted to reviewing abundance and source mechanisms of H_2 and H_2S in volcanic gases. Also, estimates of global H_2 and H_2S fluxes from subaerial volcanism remain subject to large uncertainties, owing to the sparse and limited dataset existing. For example, although natural (geogenic) H_2 emissions have received increasing

attention recently [e.g., Zgonnik, 2020], with Earth degassing being though to sustain a cumulative global H_2 flux of 6 [Gilat and Vol, 2012] to 23 [Zgonnik, 2020] Tg/yr, there are only two studies in the literature that specifically address the quantification of volcanic H_2 emissions from two persistent active volcanoes [Etna in Sicily, ~0.00065 Tg/yr; Aiuppa et al., 2011; and Erebus in Antarctica, ~0.001 Tg/yr; Moussallam et al., 2012]. As such, current inventories of volcanic H_2 fluxes to the atmosphere [0.2 to 0.7 Tg/yr; Warneck, 1988, Canfield et al., 2006, Stolper et al., 2021] are subject to large uncertainties. Likewise, the volcanogenic contribution to the global natural H_2S flux (~7.7 Tg/yr) is similarly poorly understood, with most estimates converging at ~1 Tg/yr [see review by Watts, 2000] but with total range being as large as 1 to 37 Tg/yr [Halmer et al., 2002].

Here, we review our current understanding of the processes that govern H_2 and H_2S abundance in volcanic gases. To this aim, we present an updated volcanic gas composition catalogue that we have put together from available literature information. We also use this catalogue, in combination with recently improved global volcanic SO_2 and CO_2 fluxes [Carn et al., 2017, Aiuppa et al., 2019, Fischer et al., 2019], to present an improved quantification of global volcanic H_2 and H_2S fluxes.

2. Dataset

We compiled a dataset of 747 gas analyses by complementing recent [Aiuppa, 2015, Aiuppa et al., 2017, Moussallam et al., 2019b, 2022] and older [Symonds et al., 1994, Giggenbach, 1997] volcanic gas catalogues with newly published gas results. This dataset is not exhaustive, e.g., it is not meant to cover the entire mass of information present in the geological literature. Yet, we are confident our dataset is well representative of the compositional range of volcanic gases globally (see below).

The full dataset is available as Supplementary Tables 1 and 2. The dataset includes data for both high temperature (T > 600 °C; Supplementary Table 1) magmatic gases and for lower temperature ($T \leq$ 600 °C; Supplementary Table 2) mixed (magmatic–hydrothermal) fluids. The 600 °C threshold, although somewhat arbitrary, is justified by the statistical distribution of the global volcanic arc gas population [Aiuppa et al., 2017], and is consistent with the threshold used in similar recent studies [Moussallam et al., 2019b, 2022]. Some hydrothermal (temperature close to boiling) gas samples are also used but are limited to those volcanoes that have recently erupted and/or that have detectable SO_2—this latter gas is typically absent in hydrothermal fluids "strictu sensu", that are covered by other reviews [e.g., Giggenbach, 1980, 1987, Chiodini and Marini, 1998, Fischer and Chiodini, 2015, Stix and de Moor, 2018]. The dataset is further categorised depending on tectonic setting in arc and non-arc volcanic gases, the latter including gases released by intraplate and continental rift volcanism [Aiuppa et al., 2021]. The Etna magmatic gases are plotted separately in view of the relatively enigmatic nature of volcanism at this specific locality.

The dataset combines compositional data for both fumaroles (Sample type "F" in Supplementary Tables 1 and 2) and for atmospheric gas plumes (Sample type "PL" in Supplementary Tables 1 and 2). We refer to the original studies (data sources in Supplementary Tables 1 and 2) for details on sampling and analytical procedures. Broadly speaking however, fumarole data (F) have been obtained by direct sampling (Sample Methodology "DS" in Supplementary Tables 1 and 2) [Symonds et al., 1994], in which fumarolic effluents are captured in-pre-evacuated gas flasks partially filled with a reactive solution [a NaOH solution in most applications; Giggenbach, 1996]. Incondensable gases (like H_2) are concentrated in the head space (later analysed in the lab. via Gas Chromatography), while condensable gases (such as H_2S) trapped by the solution are analysed by wet chemistry methods (typically by ion chromatography). Uncertainty in DS-derived gas concentrations is typically low (<5% in most studies). Plume results (PL) are based on in-situ, near real-time gas concentration measurements with the Multi-GAS (Sample Methodology "MG" in Supplementary Tables 1 and 2), a widely used multi-sensor unit that analyses H_2 and H_2S (among other species) with specific electrochemical sensors [Aiuppa et al., 2005, Shinohara, 2005]. In such a case, the Multi-GAS measured in-plume concentrations have been converted in air-free gas concentrations listed in Supplementary Tables 1 and 2. Typical associated uncertainty is ≤15–20%.

It is important to remind that, where available, magmatic gas compositions are reported in the form

of "restored" magmatic gas compositions at equilibrium temperature (identified by Sample type "F, R" in Supplementary Table 1). These restored gas compositions have been extracted mostly from Symonds et al. [1994], and have been obtained by the authors by applying (to measured fumarolic gas compositions) the procedure introduced by Gerlach [1993a]. This numerical procedure (i) identifies the causes of disequilibrium in volcanic gases (often due to sampling/conservation artefacts; e.g., air addition and oxidation), and (ii) iteratively removes the cause(s) of disequilibrium until an restored equilibrium gas (at a given equilibrium temperature) is obtained [Gerlach, 1993a, Symonds et al., 1994].

Our dataset, illustrated in a $H_2O/10$–CO_2–$5{\cdot}S_T$ space (where S_T is total sulphur, or $SO_2 + H_2S$) (Figure 1), demonstrates the large heterogeneity of volcanic gas compositions found in previous inventories [e.g., Symonds et al., 1994, Aiuppa, 2015], and represents well the well-established [e.g., Symonds et al., 1994, Gerlach, 1982] chemical diversity between arc and within-plate/rift magmatic gases, with the former being typically more hydrous [e.g., Fischer, 2008, Taran and Zelenski, 2015] and the latter extremely variable in terms of their CO_2/S_T signatures [e.g., Aiuppa et al., 2021]. The two magmatic gas populations exhibit some overlap, as previously found [e.g., Aiuppa, 2015]. The lower temperature ($T \leq 600$ °C) mixed gases are even more compositionally heterogeneous (Figure 1), and while many gas samples overlap with the magmatic gas range, many others plot in the CO_2-rich, S-poor compositional domain (top left portion of Figure 1), indicating some extent of sulphur loss [scrubbing; Symonds et al., 2001] during gas–water–rock hydrothermal interactions in the subsurface [e.g., Aiuppa et al., 2017].

3. Results

3.1. *Hydrogen and hydrogen sulphide abundances in volcanic gases*

H_2 and H_2S are usually minor (<1 mol%) to trace (<0.1 mol%) components of volcanic gases [e.g., Giggenbach, 1996], although H_2 concentrations exceeding 10 mol% have occasionally also been reported [see review of Zgonnik, 2020] and H_2S becomes increasingly important (e.g., a major species, >1 mol%) in low temperature hydrothermal steam samples [e.g., Giggenbach, 1980, 1997].

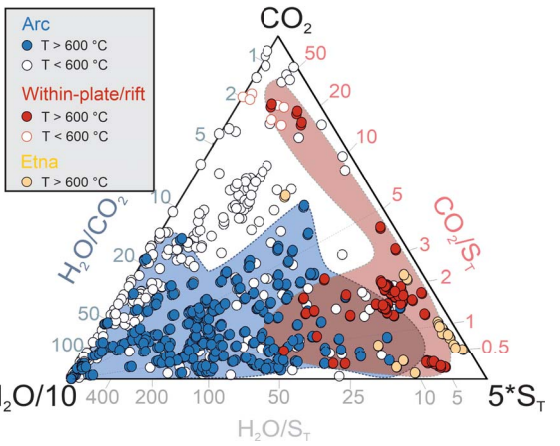

Figure 1. Triangular plots illustrating the compositional variability in the gas catalogue used (data from Supplementary Tables 1 and 2).

In our volcanic gas catalogue, H_2 and H_2S concentrations span several orders of magnitude, from ultra-trace ($<10^{-6}$ mol%) to major (>1 mol%) levels (Supplementary Tables 1 and 2). In Figures 2a and b, the whole H_2 and H_2S concentration dataset (in mol%) is illustrated as a function of measured gas outlet temperature.

Figure 2a shows that volcanic gas H_2 concentrations exhibit a marked temperature dependence, particularly at $T > 600$ °C. H_2 concentrations are the highest (0.49–3.1% levels) in the hot ($T > 1000$ °C) magmatic gases [Gerlach, 1979, 1980, 1982, 1993a,b, Symonds et al., 1994] from within-plate (e.g., Kilauea) and continental rift (e.g., Nyiragongo, Erta Ale) volcanoes. In arc magmatic gases, H_2 concentrations decrease with decreasing temperature, from 0.1–1.7 mol% at 800–1100 °C to 0.002–0.38 mol% at ~600 °C. Etna's magmatic gases plot at the boundary between arc and non-arc gases (H_2 range: 0.14–2.1 mol%). The temperature dependence is more scattered in mixed (magmatic–hydrothermal) gases, in which H_2 varies from as low as 4×10^{-6} mol% to as high as 0.867 mol%. Close-to-boiling fumaroles ($T < 100$ °C) are especially diverse in their H_2 contents that span more than 5 orders of magnitude.

H_2S concentrations show no obvious temperature dependence in the global volcanic gas catalogue (Figure 2b). The H_2S-richest samples are again found in the "restored" magmatic gas analyses from within-plate and continental rift volcanoes (H_2S range: 0.04–3.2 mol%; mean 0.9 ± 0.55 mol%). The range of H_2S

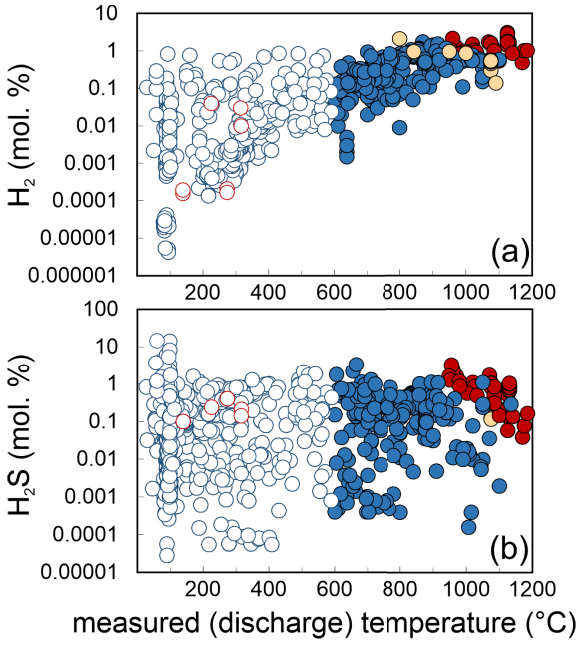

Figure 2. Scatter plots illustrating the dependence of (a) H_2 and (b) H_2S concentrations on measured discharge temperature (data from Supplementary Tables 1 and 2). Symbols as in Figure 1. In this and following figures, error bars are not shown as smaller than the data symbols.

concentrations in arc magmatic gases is vast, from 0.00016 to 3.3 mol%. The mean arc gas H_2S concentration (0.25 ± 0.55 mol%) is lower than for non-arc volcanic gases (0.9 ± 0.55 mol%), but given the large spread of values the two populations are essentially overlapping. Colder ($T \leq 600$ °C) magmatic–hydrothermal gases exhibit an even larger range of values, including the lowest (0.000028 mol%) and highest (14 mol%) values of the entire dataset. As for arc magmatic gases, no obvious pattern with temperature is observed (Figure 2a).

4. Discussion

4.1. *Ratios between redox couples*

A standard practise used when interpreting volcanic gas H_2 and H_2S concentrations is to normalise them to their oxidised counterparts H_2O and SO_2 [Gerlach, 1980, Giggenbach, 1996, 1987]. This practise developed on since early demonstrations [Ellis, 1957, Matsuo, 1962] that high temperature volcanic gases approach a state of thermodynamic equilibrium, in which ratios between redox couples are controlled by equilibria:

$$H_2 + \tfrac{1}{2}O_2 = H_2O \quad (1)$$

$$H_2S + \tfrac{3}{2}O_2 = SO_2 + H_2O \quad (2)$$

In a set of seminal articles, Gerlach and co-workers [Gerlach, 1979, 1980, 1993a,b, Symonds et al., 1994] confirmed that the assumption of "full" equilibrium among all the different species in a volcanic gas mixture holds at magmatic temperatures. A useful concept introduced to test this full equilibrium state hypothesis was that of the so-called Correspondence Temperature (CT), the temperature at which the measured (in a specific volcanic gas sample) and equilibrium concentrations of a gas species match one another. As the CTs of the different gas species were found to converge to within a very narrow range in many high temperature gas samples [Gerlach, 1979, 1980, 1993a,b], the full equilibrium hypothesis could be proved.

However, as demonstrated in later work by Giggenbach [1987, 1996], the full equilibrium assumption is unlikely to hold in lower temperature gas samples, where different extents of re-equilibrations of the different redox couples (e.g., reactions (1) and (2)), as well as admixing with external (meteoric, atmospheric) fluids [Taran and Zelenski, 2015] and reaction with wall-rocks [Henley and Seward, 2018, Henley and Fischer, 2021], become likely eventualities. In such conditions, a conservative approach is to deal with specific redox reactions individually, e.g., to use plots that compare, for each specific redox couple, the analytically determined and equilibrium ratios. This approach, initially elaborated by Giggenbach [1987, 1996] and Chiodini et al. [1993], is followed below, where we update their results and corroborate their conclusions using the more complete, today available gas catalogue (Supplementary Tables 1 and 2).

At discharge conditions ($P = 1$ bar), and at equilibrium, reactions (1) and (2) imply that ratios between redox couples will exhibit the following dependences on redox (as expressed by oxygen fugacity, fO_2) and temperature (in K):

$$\log \frac{H_2}{H_2O} = -\frac{12{,}707}{T} + 2.548 - \frac{1}{2}\log fO_2 \quad (3)$$

$$\log \frac{SO_2}{H_2S} = \frac{27{,}377}{T} - 3.986 + \frac{3}{2}\log fO_2 - \log X_{H_2O} \quad (4)$$

These equations are obtained by re-arranging the equilibrium constants K_1 and K_2 of (1) and (2) [we use thermodynamic data from Chase and National Institute of Standards and Technology (U.S.), 1998] and assuming ideal gas behaviour (fugacity coefficients $\gamma = 1$).

The presence of redox sensitive elements in either the silicate melt/rock matrix (where iron is typically available in both +2 and +3 valence states) or in the gas phase (where sulphur is present in sufficient amounts in both −2 and +4 valence states) has long been proposed [e.g., Giggenbach, 1987, Gerlach, 1993a] to act as a buffer for oxygen fugacity in volcanic gases [see Moretti and Stefánsson, 2020, Moretti, 2021, Moretti and Neuville, 2021, for examples of recent reviews]. Gerlach [1993a,b] proposed that gas speciation in high temperature (>900 °C) magmatic gases is buffered by equilibrium redox exchange between gas and coexisting silicate melt. The same buffers can also operate at sub-solidus conditions, e.g., if gas reacts and equilibrates with the host rock matrix in which iron is present in minerals with two distinct oxidation states [e.g., Giggenbach, 1987]. It was however found that, in such lower temperature conditions, the buffering role of sulphur in the gas phase (where H_2S and SO_2 are simultaneously present) becomes increasingly effective [e.g., Giggenbach, 1987, 1996], although the competing roles of homogeneous (gas-only) and heterogenous (gas–mineral) reactions in controlling the volcanic gas redox budget remained debated [e.g., Henley and Fischer, 2021] (see below).

Irrespective of the buffering medium (either melt, rock, or gas), fO_2 in (3) and (4) can conveniently be replaced by the temperature dependences imposed by the redox buffers [e.g., Eugster, 1977, Frost, 1991, see recent reviews by Cicconi et al. [2020], Moretti and Neuville [2021]]. The predicted (3), mineral-buffered or gas-(H_2S/SO_2) buffered, H_2/H_2O ratios are graphically illustrated in Figure 3a. The same mineral buffered SO_2/H_2S ratios are illustrated in Figure 3b. These model trends implicate that, in mineral-buffered conditions (e.g., when gas redox is buffered by heterogeneous redox budget exchanges with either the melt or the host rocks), H_2 is expected to become increasingly abundant (relative to H_2O), and H_2S increasingly depleted (relative to SO_2), with increasing temperature (Figure 3). At fixed temperature, H_2/H_2O ratios are expected to decrease (and SO_2/H_2S to increase) as redox evolves from more reducing (e.g., redox buffered at the Fayalite–Magnetite–Quartz (FMQ) mineral buffer) to more oxidised (as expressed by the hematite–magnetite (HM) mineral buffer) conditions. Results of a comparison between modelled and measured (volcanic gases) ratios are summarised below (Figure 3).

4.1.1. *High-temperature magmatic gases*

The measured volcanic gas H_2/H_2O ratios, as derived from the analytically determined gas concentrations, are illustrated in Figure 3a (and listed Supplementary Tables 1 and 2). Comparison with modelled compositions (see above) shows that the hot ($T > 900$ °C) non-arc magmatic gases [Gerlach, 1980, 1993b, Symonds et al., 1994] have "restored" gas compositions that convert into H_2/H_2O (and SO_2/H_2S ratios; see Figure 3b) overlapping those predicted at equilibrium (3) and (4) in a melt-buffered gas system at ~FMQ, see Figures 3 and 4. As previously found [Gerlach, 1980, 1993a,b] therefore, the H_2 and H_2S contents of such gases appear to be controlled by heterogeneous (melt–gas) redox exchanges. High temperature ($T > 900$ °C) arc magmatic gases likewise approach the melt-buffered model lines, but the majority of them plot at lower H_2/H_2O (and higher SO_2/H_2S) ratios relative to non-arc magmatic gases, close to the NNO (Nickel–Nickel-Oxide) mineral buffer model line (Figure 3). This apparent more oxidised (lower H_2/H_2O ratios) signature of arc gases is also well represented in Figure 4, and we will return to this point in later sections (cf. Section 4.3).

4.1.2. *Mixed magmatic–hydrothermal gases*

Lower temperature magmatic gases (600 °C < T < 900 °C) and mixed (magmatic–hydrothermal) gases (T < 600 °C) overall identify a compositional tendency of decreasing H_2/H_2O ratios with decreasing temperature (Figure 3a). This trend (qualitatively identified by the grey shaded region of Figure 3a) is manifestly steeper than the temperature dependences imposed by any of the mineral fO_2 buffers (solid lines). Giggenbach [1987, 1996] took this as evidence of a marginal (if any) control exercised by redox budget exchanges between gases and silicate melts (in the supra-solidus regions) and/or with wall rocks (in the sub-solidus region). Rather, Giggenbach [1987, 1996] proposed that the H_2/H_2O ratios versus temperature dependence exhibited by volcanic gas

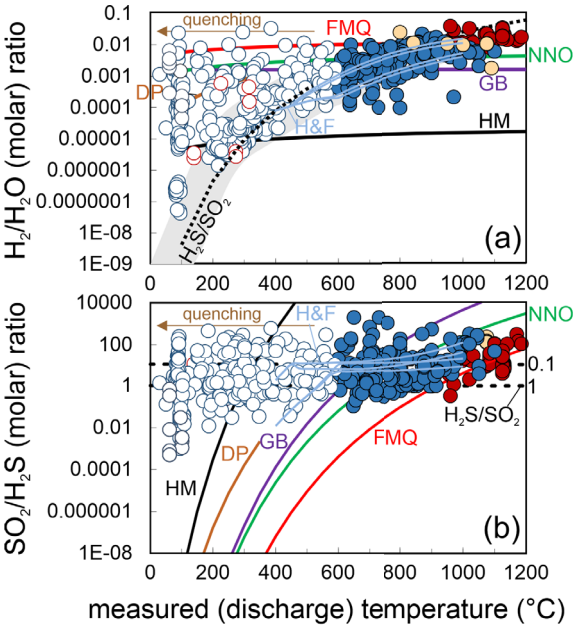

Figure 3. Temperature dependence of (a) H_2/H_2O and (b) SO_2/H_2S molar ratios in our volcanic gas catalogue (data from Supplementary Tables 1 and 2). Symbols as in Figure 1. The thick coloured lines are the predicted temperature dependences of the ratios imposed (at 1 bar) by the most common mineral and gas buffers. These are obtained by using Equations (3) and (4) and oxygen fugacity buffered by either the melt/rock matrix or sulphur species in the gas phase. The mineral buffer [see Frost, 1991, for the relevant fO_2–T relationships] curves illustrated are: HM: Hematite–Magnetite; NNO: Nickel–Nickel Oxide; FMQ: Fayalite–Magnetite–Quartz; GB: FeO–$FeO_{1.5}$ buffer [Giggenbach, 1987]. The dashed line in (a) labelled H_2S/SO_2 corresponds to the sulphur gas buffer of Giggenbach [1987], and is obtained by solving Equation (6) (at 1 bar) assuming equimolar amounts of H_2S and SO_2 (H_2S/SO_2 = 1) (a similar line at fixed H_2S/SO_2 of 0.1 is also shown in panel (b)). The DP line is for gas ratios predicted using the empirically derived fO_2 versus temperature dependence typical of hydrothermal systems [e.g., D'Amore and Panichi, 1980]. Thin light blue curves labelled H&F are the gas ratios predicted by the gas–mineral reactions of Henley and Fischer [2021] (the model runs illustrated in their original Figure 5 are shown).

Figure 3. (**cont.**) The majority of the mixed (magmatic–hydrothermal; T < 600 °C) gases plot in panel (a) along a compositional array (grey dashed area) that overlaps with both (i) the H_2S/SO_2 buffer lines, and (ii) the heterogenous (gas–mineral) equilibria of Henley and Fischer [2021]. Many gas samples have higher H_2/H_2O ratio compositions than predicted by either homogenous [Giggenbach, 1987] or heterogeneous [Henley and Fischer, 2021] reactions, likely indication preservation (quenching) of higher-T equilibria. High-T magmatic gases plot in between the NNO and FMQ mineral buffers, suggesting buffering from source silicate melt. See text for discussion.

samples (Figure 3a) can satisfactory be explained by homogeneous (gas-phase only) redox reactions taking place during gas expansion and cooling, according to reaction:

$$3H_2 + SO_2 = 2H_2O + H_2S \quad (5)$$

from which:

$$\mathrm{Log}\frac{H_2}{H_2O} = -\frac{1}{3}\mathrm{Log}\,K_5 + \frac{1}{3}\mathrm{Log}\frac{H_2S}{SO_2} - \frac{1}{3}f_{H_2O} \quad (6)$$

The basic principle behind Equations (5)–(6) is that the gas H_2/H_2O ratio will re-adjust (re-equilibrate) as temperature decreases (e.g., during gas ascent and adiabatic expansion from source (magma) to atmospheric discharge) in a gas-buffered regime in which H_2S–SO_2 coexistence will control the gas redox budget. Equation (6), at 1 bar and for equimolar amounts of H_2S and SO_2 (H_2S/SO_2 = 1), resolves into what Giggenbach [1987, 1996] referred as the H_2S/SO_2 gas buffer (Figure 3).

The resulting model-derived (Equation (6)) temperature dependence of the H_2/H_2O ratios (dashed line labelled H_2S/SO_2; Figure 3a) nicely reproduces the volcanic gas compositional array (grey band). Notably, this ability of coexisting H_2S and SO_2 to buffer gas phase redox is entirely consistent with the temperature invariant, analytically determined SO_2/H_2S ratios (Figure 3b). Giggenbach [1987] concluded that the conversion of SO_2 to H_2S during gas cooling, as implicated by the mineral buffer curves (Figure 3b), is inhibited by the rapid transit of magma sourced gases through host rocks, preventing gas–rock reactions to become effective (to achieve equilibrium).

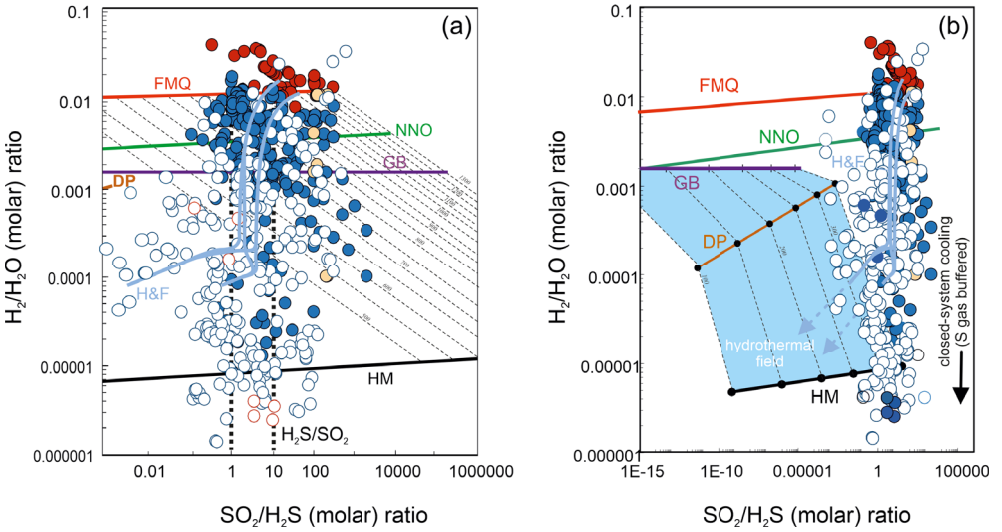

Figure 4. (a) Scatter plot of SO_2/H_2S versus H_2/H_2O molar ratios in our volcanic gas catalogue (data from Supplementary Tables 1 and 2). Symbols as in Figure 1. The thick coloured lines are the predicted gas molar ratios (from Equations (3) and (4)) for fO_2s calculated using the temperature dependences imposed by the FMQ, NNO, GB and HM mineral buffers (calculations are run over a range of temperatures, as expressed by the isotherms: dashed lines, in °C). The DP line is derived by using (for fO_2 in Equations (3) and (4)) the empirical fO_2 versus T dependence in hydrothermal systems [D'Amore and Panichi, 1980]; thin light blue curves labelled H&F are the gas ratios predicted by the gas–mineral reactions of Henley and Fischer [2021] (the model runs illustrated in their original Figure 5 are shown). (b) An expanded version of (a) illustrating the nominally SO_2-free field of hydrothermal steam samples (in the 100–350 °C temperature range). The magmatic to mixed (magmatic–hydrothermal) samples in our catalogue, having detectable SO_2, plot to the right of the hydrothermal field. Their SO_2/H_2S versus H_2/H_2O population is well reproduced by both homogenous [gas-phase only; dashed black lines; Giggenbach, 1987] or heterogeneous [Henley and Fischer, 2021] reactions. However, the H&F models predict progressively decreasing SO_2/H_2S ratios at increasing mineral–gas reactions (and with decreasing temperatures), while the majority of the gas samples define a vertical array that is more consistent with gas oxidations (e.g., decreasing H_2/H_2O ratios) during closed-system gas cooling in a S gas-buffered regime [dashed vertical back line, the H_2S/SO_2 gas buffer of Giggenbach, 1987].

The temperature-invariant, measured SO_2/H_2S gas compositions in our dataset (Figure 3b) indeed suggest that sulphur speciation is little affected by gas–mineral reactions during cooling, although data align along a nearly horizontal trend at SO_2/H_2S of ~10 (H_2S/SO_2 of ~0.1) rather than ~1 [as implicated in the original H_2S/SO_2 gas buffer of Giggenbach, 1987, 1996] (Figures 3b, 4).

An alternative view to that of Giggenbach [1987] has recently been proposed by Henley and Fischer [2021]. The authors, based on field evidence arising from rock alteration assemblages found at extinct (now eroded) andesitic volcanoes [Henley and Berger, 2011, Henley et al., 2015], proposed that gas H_2/H_2O and SO_2/H_2S ratios are controlled by heterogeneous (mineral–gas) rather than homogenous (gas-only) reactions. The authors presented a comprehensive multi-component thermochemical modelling of gas–solid equilibria of magmatic SO_2 reaction with primary rock-forming minerals. The key reaction invoked by the authors is:

$$CaAl_2Si_3O_{8(s)} + 2SO_{2(g)} + 2H_{2(g)} = CaSO_{4(s)} + Al_2SiO_{5(s)} + SiO_{2(s)} + H_2O_{(g)} + H_2S_{(g)} \quad (7)$$

in which magmatic SO_2 disproportionate into both oxidised (anhydrite) and reduced (H_2S) sulphur forms while plagioclase is converted into a secondary

Al-bearing hydrothermal mineral. Similar reactions can be written to account for the reaction of magmatic SO_2 with ferromagnesian minerals, such as ferrosilite (Fe-rich pyroxene) [Henley and Fischer, 2021]:

$$FeSiO_{3(s)} + SO_{2(g)} + 3H_{2(g)} = FeS_{(s)} + 3H_2O_{(g)} + SiO_{2(s)} \quad (8)$$

This reaction nicely accounts for the pervasive precipitation of iron sulphides (e.g., pyrite and pyrrhotite) in hydrothermal systems.

The equilibrium constant of reaction (7):

$$K_7 = \frac{H_2S}{SO_2} \cdot \frac{1}{SO_2} \cdot \frac{1}{H_2O} \cdot \frac{1}{\left(\frac{H_2}{H_2O}\right)^2} \quad (9)$$

was rearranged by Henley and Fischer [2021] to obtain:

$$\mathrm{Log}\frac{H_2S}{SO_2} = \mathrm{Log}\,K_7 + 2\,\mathrm{Log}\frac{H_2}{H_2O} + \mathrm{Log}\,S_T - \mathrm{Log}\left(K_5 \cdot \left(\frac{H_2}{H_2O}\right)^3 P_{\mathrm{tot}} + 1\right) \quad (10)$$

Equation (10) demonstrates that SO_2-mineral reactions can control both gas composition and redox state (e.g., H_2/H_2O and SO_2/H_2S and Total gas phase sulphur, S_T) at a given total pressure (P_{tot}). Figures 3 and 4 illustrate examples of such gas–mineral reaction paths (light blue lines labelled H&F). The plotted model curves [we illustrate the example runs shown in the original Figure 5 of Henley and Fischer, 2021] are representative of closed-system multi-component (mineral–gas) equilibrium runs in a range of pressures (either 1 or 100 bars), gas–mineral ratios (either 10 or 100) and temperatures (400–1000 °C), and highlight the expected gas compositional changes in such gas–mineral reaction environments. The model reaction paths derived by Henley and Fischer [2021] indicate that, as reaction progresses (e.g., while gases increasingly react with host-rock minerals during their ascent, expansion and cooling), the H_2/H_2O, SO_2/H_2S and S_T are all expected to decrease in the residual gas phase (8). The H&F model lines satisfactorily reproduce the observed (volcanic gas) H_2/H_2O temperature dependence (Figure 3a). In the models, the predicted SO_2/H_2S ratios are relatively invariant in the 1000–600 °C temperature range, but then drop at <600 °C as SO_2 is increasingly converted into H_2S and sulphates/sulphides (8) and (9) (Figures 3b and 4).

If either homogeneous (gas-only; Equation (5)) or heterogenous (gas–mineral; Equations (7)–(8)) reactions prevail (during ascent and cooling of magmatic gases from source to surface) cannot be unambiguously resolved from our model versus natural samples comparison. In principle, there is no reason to exclude both reaction mechanisms can indeed co-operate in a volcanic system in space and time. The heterogeneous (gas–mineral) reactions satisfactorily explain the transition of magmatic gases into nominal SO_2-free hydrothermal gases (dashed light blue arrows in Figure 4b), and are expected to prevail in mature hydrothermal systems where the transit of gas is sufficiently slow to insure gas–mineral titration effectively takes place, leading to SO_2-to-H_2S conversion and sulphur loss to hydrothermal minerals. In more active magmatic systems, vice versa, it is well possible that gas transit through the host rocks is fast enough to prevent large SO_2 scavenging from reactions with minerals. Our mixed (magmatic–hydrothermal) gases all contain detectable SO_2, and the SO_2/H_2S ratios are relatively temperature invariant (Figures 3b and 4a,b), implying the gas may remain closed to reactions with host rocks in many cases, in which case reaction (5) would keep a major control on gas chemistry and redox.

Neither homogeneous nor heterogenous reactions can explain the high H_2/H_2O ratio signature of many relatively low-temperature (T < 400 °C) gas samples (Figure 3a). These H_2-rich compositions imply that re-equilibration (upon gas cooling) may eventually not take place at all, causing the surface discharge of relatively cold gases to preserve quenched, higher-temperature equilibrium conditions (see arrow labelled "quenching" in Figure 3). Ultimately, the extent of (gas or gas–mineral) re-equilibration will range from minimal to total in natural systems, depending on the local conditions and specific ascent/cooling histories of gases, as on their route to the surface.

4.2. *Use of hydrogen and hydrogen sulphides as geothermometers*

The strong temperature dependence of H_2 concentrations (Figure 2a) and H_2/H_2O ratios (Figure 3a), combined with relatively temperature-invariant SO_2/H_2S ratios (Figures 3b, 4a,b), suggest that gas chemistry and redox are often internally buffered (by the gas-phase reaction (5)). One possible way to test if/to what extent fast-reacting H_2 rapidly attains equilibrium in an internally buffered volcanic gas

phase (e.g., whose redox is controlled by the H_2S–SO_2 gas buffer) is to use Equation (5) to estimate Apparent Equilibrium Temperatures [AETs; e.g., Matsuo, 1962, Ohba et al., 1994, Moussallam et al., 2019b, 2022], and compare these with measured (discharge) temperatures. Deriving such AETs from measured H_2, H_2O, SO_2 and H_2S compositions [e.g., Moussallam et al., 2019b, 2022] is especially important at open-vent volcanoes [Shinohara et al., 2011, 2015, 2018], in which gas observations are typically taken in "cold" atmospheric volcanic gas plumes, whose source vents are inaccessible to direct temperature measurements [this contrasts with closed-conduit volcanoes in which gas venting temperatures are measured concurrently with gas sampling at the fumarolic outlet; e.g., Ohba et al., 1994]. Such information on magma source temperatures can be recorded in the composition of the plume at condition that gas-melt equilibria (i) are established at magma T–P-redox conditions, and (ii) conserved during gas cooling and mixing during atmospheric dispersion. Assumption (ii) is indeed verified by observations/models that suggest quenching of magmatic gas composition in volcanic plumes [in which source H_2/H_2O and SO_2/H_2S ratios are conserved during plume aging; Aiuppa et al., 2007, 2011].

Our gas catalogue here offers an opportunity to test condition (i) above and, ultimately, to verify if internal (gas-phase) redox buffering prevails in magmatic systems (over heterogeneous reactions).

We initially illustrate in Figure 5a the temperature dependence of the equilibrium constant of reaction (5) (expressed in the form of $\mathrm{Log}\,K_5$), as derived from thermodynamic data in Ohba et al. [1994]. This equilibrium line (solid black line in Figure 5a) is contrasted against analytical values of $\mathrm{Log}\,K_5$, as derived by solving (for each sample in Supplementary Tables 1 and 2) Equation (6) using analytically determined H_2/H_2O and H_2S/SO_2 ratios (water fugacity, fH_2O, is calculated from measured X_{H_2O} and assuming 1 bar total pressure and ideal gas behaviour). This comparison shows that the "restored gas analyses" output analytical $\mathrm{Log}\,K_5$ values that perfectly overlap with the equilibrium curve: this merely reflects the accuracy of the gas restoration procedure of Gerlach [1980]. More significant is the observation that unrestored magmatic gases (600 °C < T < 1100 °C) have analytically determined $\mathrm{Log}\,K_5$ that match closely equilibrium $\mathrm{Log}\,K_5$ values: for these samples, approach to equilibrium is proved by the close match between measured (discharge) temperatures and AETs (Figure 5b). Some mixed hydrothermal-magmatic gases also plot along (or at least very close to) the model equilibrium curve (Figure 5a), indicating that equilibrium conditions can still be achieved during gas cooling at temperatures of <600 °C (and as low as ~200 °C; Figures 5a, b). However, in such a temperature range, and increasing number of samples output analytically derived $\mathrm{Log}\,K_5$ that diverge from the equilibrium line (Figure 5a): in these samples, AETs exceed measured (discharge) temperatures by several hundred degrees in some cases, again indicating quenching of higher temperature (magmatic) conditions, and or disequilibrium conditions. These are the same samples that in Figure 3a diverge from the main compositional-temperature array (grey band) toward higher H_2/H_2O ratios.

The conclusion we can take is that, as previously shown by Moussallam et al. [2019b] (see their Figure S1), at magmatic temperatures (>600 °C), gas compositions can allow estimating AETs that are within ±20% of actual venting temperatures (Figure 5d). It is very interesting to realise however that even at lower (<600 °C) gas venting temperatures, quenching of higher temperature compositions, or disequilibrium conditions, is indeed common.

The calculations above do not necessarily imply that gas–mineral reactions (7)–(8) are altogether unimportant. Reactions between gas and host-rocks [e.g., Symonds et al., 2001, Henley and Fischer, 2021] are central to the formation of SO_2-poor hydrothermal steam samples [e.g., Giggenbach, 1980]. In the 600 °C < T < 1200 °C temperature range however, the fraction of SO_2 loss via reaction (7) and (8) is overall a limited fraction (of the total S load in the gas phase), thus exercising little to no effect on gas equilibria (Figure 5).

4.3. *Use of hydrogen and hydrogen sulphides to estimate oxygen fugacity*

A matter that has remained debated for years is if, and to what extent, volcanic gas compositions reflect (and can therefore allow deriving) the redox conditions (oxygen fugacities) of the source magmas.

Gerlach [1982] found that their "restored" magmatic gas analyses from tholeiitic and alkaline intraplate volcanoes allow calculating gas oxygen fugacities that vary from ~$10^{-8.5}$ to ~10^{-12} bar. He also

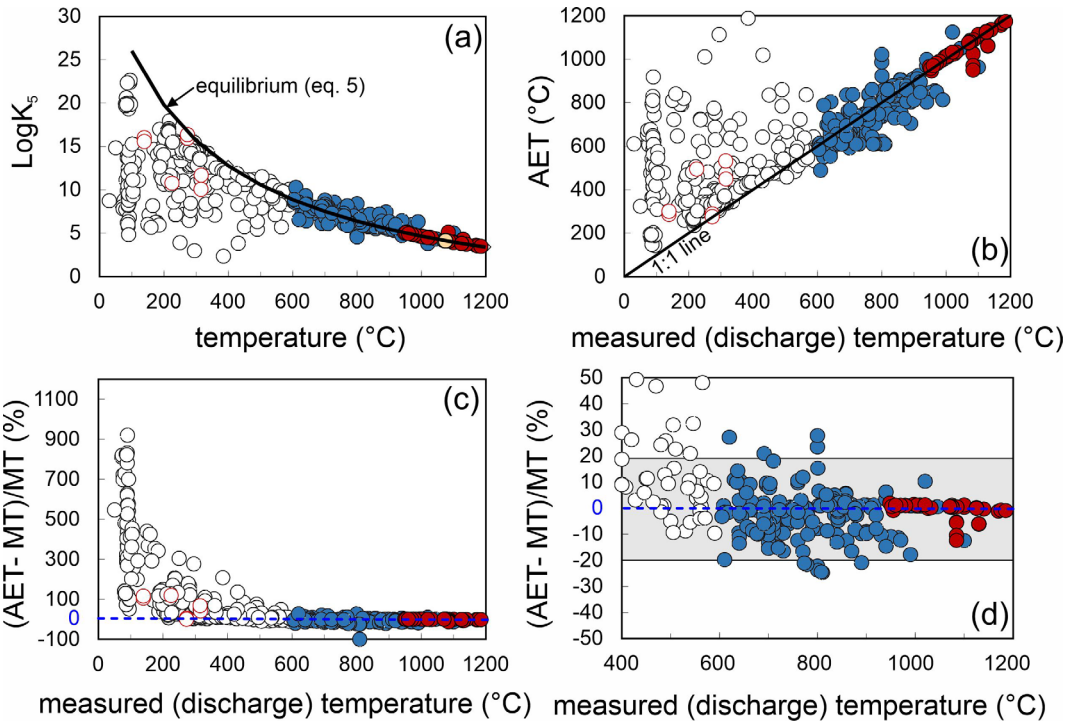

Figure 5. (a) Temperature dependence of the equilibrium constant of reaction (5) (expressed in the form of LogK_5), as derived from thermodynamic data in Ohba et al. [1994]. The equilibrium line (solid black line) is contrasted against analytical values of LogK_5, as derived by solving (for each sample in Supplementary Tables 1 and 2) Equation (6) using analytically determined H_2/H_2O and H_2S/SO_2 ratios (water fugacity, fH_2O, is calculated from measured XH_2O and assuming 1 bar total pressure and ideal gas behaviour). (b) Apparent equilibrium temperatures (AET) [Matsuo, 1962, Ohba et al., 1994, Moussallam et al., 2022] derived from Equation (6) and analytically determined H_2/H_2O and H_2S/SO_2 ratios for individual gas samples. High-temperature gases plot along the 1:1 line, e.g., they match closely measured discharge temperature (x-scale), implying equilibrium conditions. (c) The difference between Apparent equilibrium temperatures (AET) and measured temperatures (MT) approach 0 in high-T gas samples, while AETs exceed MTs at lower temperatures (implying quenching of higher-T equilibria. (d) A magnified version of (c), demonstrating AET and MT differ by $< \pm 20\%$ at $T > 600$ °C.

found these fO_2 values to be strongly temperature dependent, and to overall define a fO_2-collection temperature trend parallel to the fO_2–T dependence imposed by the Fayalite–Magnetite–Quartz (FMQ) and Nickel–Nickel Oxide (NNO) redox buffers [Eugster, 1977, Frost, 1991]. From this, he concluded that "*... lavas tend to buffer the O_2 fugacities of their associated gases*". Confirmation to this hypothesis came from later studies [Gerlach, 1993a,b] in which the fO_2 values for (restored) magmatic gases from Kilauea were found to match the measured/calculated fO_2 values of Kilauea basalts. Again, Gerlach [1993a] concluded that "*the evidence discussed above indicates that subaerial lavas buffer volcanic gas compositions emitted by Kilauea basalt along consistent fO_2-T trend from molten to subsolidus temperatures*". A strong temperature dependence of volcanic gas fO_2 values was also found in the global compilation of Symonds et al. [1994].

This "melt-buffering" hypothesis has recently been challenged in a series of studies by Oppenheimer et al. [2018] and Moussallam et al. [2019b, 2022] using evidence from novel gas plume observations, either in-situ or remote. Using results from

Open Path Fourier Transform Infra-Red (OP-FTIR) spectroscopy observations of lava lake degassing at Kilauea volcano, Oppenheimer et al. [2018] found that gas composition varies with activity style and temperature. They found, in particular, that the volcanic gas phase becomes progressively oxidised as gas temperature progressively drops (below magmatic temperature), at a rate that is inconsistent with that predicted by external gas redox buffering by the coexisting silicate melt. They proposed that magmatic gas redox (fO_2) is controlled by homogeneous (gas-phase only) redox re-equilibration upon adiabatic gas cooling. Using evidence from a global volcanic gas dataset, Moussallam et al. [2019b] generalised the conclusions of Oppenheimer et al. [2018], showing that the temperature dependence of volcanic gas fO_2 is different (less steep) than that imposed by external melt redox buffers. Rather, they found that volcanic gas redox scales with the extent of gas cooling experienced by gases (as indicated by temperature difference between gas and the source melt). In this interpretation therefore, volcanic gas redox decouples from that of the melt, i.e., the melt redox information is altered in the gas during its adiabatic cooling (as gas bubbles separately rise within—and ultimately burst out of—the silicate melt). To capture this concept, Moussallam et al. [2022] proposed the use of the formulation "apparent oxidation state" or AOS which is the oxidation state of the gas mixture at its apparent equilibrium temperature. Moussallam et al. [2022] showed that if the magma temperature is known then the gas AOS can be restored to its true fO_2 at equilibrium with the magma (i.e., the oxidation state of the magma can be calculated from the AOS).

Hydrogen and hydrogen sulphide are inherently central to this discussion, as Equations (3) and (4) can conveniently be re-arranged to estimate AOS from measured/apparent temperature and either H_2/H_2O or SO_2/H_2S ratios. Figure 6a is a plot of derived fO_2 values for gas samples in our catalogue, as derived from Equation (3) using measured H_2/H_2O ratios and AETs. fO_2s obtained by SO_2/H_2S ratios (and Equation (4)), also listed in Supplementary Tables 1 and 2, agree well with those derived from H_2/H_2O ratios. The whole volcanic gas population defines in Figure 6a a roughly linear temperature-fO_2 array which slope is manifestly less steep than that of any mineral buffer line. Overall, the volcanic gas population span from redox conditions between the NNO and FMQ buffers at temperatures of 900 °C or more, to redox close to the Hematite–Magnetite (HM) buffer at the low temperature (<400 °C) end of the population. Our results thus corroborate the results of Moussallam et al. [2019b, 2022] that volcanic gases become increasingly oxidised with decreasing temperatures. The high temperature (T > 600 °C) magmatic gas field is magnified in Figure 6b.

We modelled the closed-system cooling of three gas compositions from Erta' Ale [Le Guern et al., 1979], Satsuma-Iwojima [Shinohara et al., 1993] and Etna [Aiuppa et al., 2011]. The calculation method is detailed in Moussallam et al. [2019b, 2022] and results are shown in Figure 6b. This shows that even at low (<600 °C) temperature the oxidation state of volcanic gases having suffered limited interaction with the hydrothermal system can be explained by closed system cooling from magmatic temperature. This is an astonishing and very fortunate finding as it means that volcanic gases with AET as low as a few hundred degrees might preserve information of the oxidation state and/or temperature of the magma from which they escaped by simply applying the gas restoration calculations described in Moussallam et al. [2022]. For example, we can perform the same calculations but this time starting with the measured gas composition from Kawa Ijen volcano collected by Allard 1985 at a measured temperature of 244 °C but with an AET of ~343 °C and at an AOS at QFM+5. Restoring [using Moussallam et al., 2022] the volcanic gas composition back to a magmatic temperature (arbitrarily set to 1000 °C for the purpose of demonstration) would lead to a restored gas composition with an oxidation state and magmatic temperature of QFM+0.3.

The link between volcanic gas and silicate melt (magma) redox is more fully analysed in Figure 7. Figure 7a is a frequency distribution diagram of derived (Equation (3)) apparent oxygen fugacities for magmatic gases (temperature > 600 °C). The figure demonstrates distinct redox conditions for non-arc and arc volcanic gases. In spite of some overlap, most arc volcanic gases have apparent fO_2s (as expressed as $\Delta FMQ = \log fO_{2(\text{sample})} - \log fO_{2(\text{FMQ at AET})}$) at $\Delta FMQ \geq 0$, and as high as $\Delta FMQ + 4$; whilst non-arc volcanic gases are generally more reduced $\Delta FMQ \leq 0.2$, and as low as $\Delta FMQ - 1.2$. This diversity is largely explained by the arc gas dataset containing many

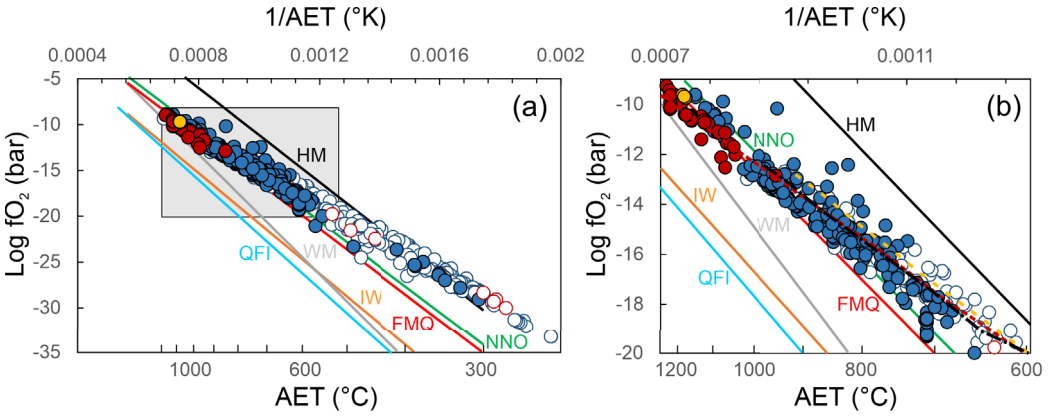

Figure 6. The temperature dependence of volcanic gas oxygen fugacities (a) apparent oxygen fugacities of individual gas samples (data from Supplementary Tables 1 and 2), as derived using Equation (2) from measured H_2/H_2O ratios and estimated Apparent Equilibrium Temperatures (AET; same as Figure 5). Calculated Log fO_2 values vary linearly with 1/AET, but the slope of the linear function is manifestly less steep than the Log $fO_2 - 1/T$ dependence imposed by the most common mineral redox buffers [HM: Hematite–Magnetite; NNO: Nickel–Nickel Oxide; FMQ: Fayalite–Magnetite–Quartz; WM: Wustite–Magnetite; IW: Iron–Wustite; QFI; Quartz–Fayalite–Iron; see Frost, 1991, Moretti and Neuville, 2021]; (b) a magnified version of (a) comparing the Log $fO_2 - 1/T$ dependence for high-temperature (>600 °C) volcanic gases. The dashed lines illustrate the gas evolution predicted from closed-system (gas cooling) calculations. The closed system model lines suitably reproduce the compositional trend (increasingly oxidised conditions upon cooling) described by natural samples.

fumarole samples in the 600–900 °C temperature range, which have therefore cooled significantly below source magma temperatures, ultimately having become more oxidised during closed-system reactions [see Figure 6 and related discussions and see Figure 1 in Moussallam et al., 2022 showing the oxidation state of arc gases restored to magmatic temperature]. However, arc gases sampled at close to magmatic temperatures ($T > 900$ °C) still plot at higher redox than non-arc magmatic gases (Figure 7a; see also Figures 4 and 6b), implying that the volcanic gas fO_2 difference is likely to reflect some distinct redox conditions at source. Intraplate (Figure 7b) and arc (Figure 7c) melts have previously been shown to exhibit distinct redox [Cottrell et al., 2022]. We conclude, therefore, that these diverse magma fO_2s are well preserved in volcanic gases, provided adiabatic cooling and re-equilibration have not occurred (e.g., at $T \gg 900$ °C). It is important to remember, however, that melt redox has been found to vary upon magma de-compressional ascent and degassing, progressively becoming more reduced [e.g., Moussallam et al., 2014a, 2016, 2019a, Brounce et al., 2017, Helz et al., 2017] at low pressure [when S(IV) is lost to gas as SO_2, leading to an overall decrease of the magma redox budget; [Evans, 2012]]. As such, magmatic gas may, at some conditions (limited adiabatic cooling), reflect redox of shallow, surface-emplaced magma; however, it is unlikely to provide information on deep magma (and source mantle) redox [Moretti and Stefánsson, 2020].

4.4. *Atmospheric fluxes*

Upon their atmospheric release from subaerial volcanoes, volcanogenic H_2 and H_2S act as primary electron donors (e.g., as reducing compounds) in the atmosphere [e.g., Holland, 2002, Canfield et al., 2006]. As these volcanic gas species thus contribute largely to the reducing power (e.g., the ability to remove atmospheric O_2) of volcanic gases, understanding their volcanic atmospheric fluxes is central to reconstructing the oxygenation history of the early atmosphere and the present atmospheric oxygen budget [Holland, 2002, Canfield et al., 2006, Stolper et al., 2021].

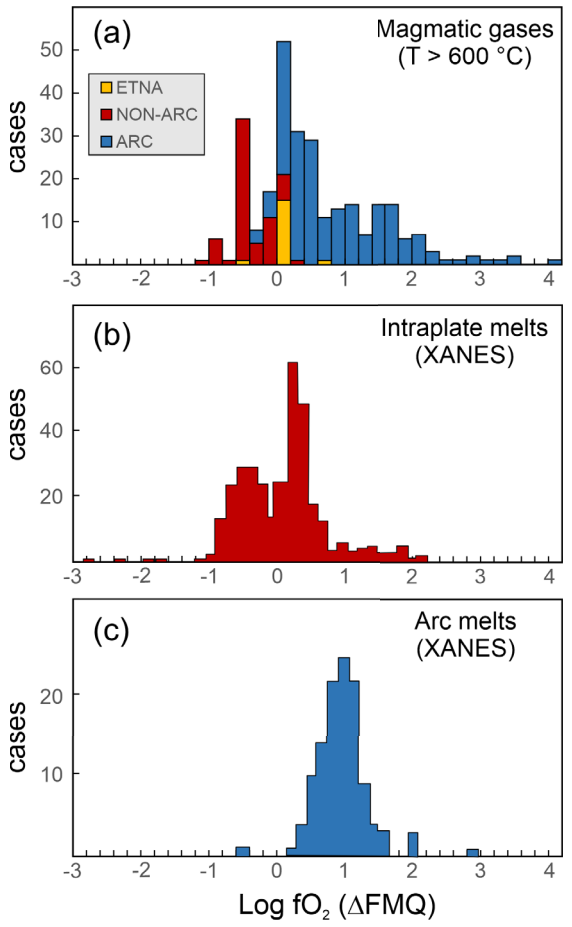

Figure 7. (a) Frequency distribution diagram of derived (Equation (3)) apparent oxygen fugacities for magmatic gases (temperature > 600 °C), expressed as $\Delta\text{FMQ} = \log fO_{2(\text{sample})} - \log fO_{2(\text{FMQ at AET})}$. The figure demonstrates distinct redox conditions for non-arc and arc volcanic gases in the same range and magnitude as seen for intraplate (panel b) and arc (panel c) melts [redrawn from Cottrell et al., 2022].

As for the more abundant CO_2 [Aiuppa et al., 2019, Werner et al., 2019, Fischer et al., 2019], the volcanic H_2 and H_2S fluxes to the atmosphere cannot be measured directly by remote sensing, as no specific observational technique exists for this aim. Therefore, although some rare direct in-situ flux measurements exist [Aiuppa et al., 2013, Allard et al., 2014, Tamburello et al., 2019, Moune et al., 2022], most applications rely on the indirect approach [Aiuppa et al., 2019, Fischer et al., 2019, Werner et al., 2019] of scaling gas ratios (H_2/SO_2 and H_2S/SO_2 ratios in this specific case) in volcanic emissions to the global volcanic SO_2 flux budget [e.g., Carn et al., 2017, Fischer et al., 2019], which is well understood thanks to abundant UV spectroscopy observations from both ground [Arellano et al., 2021] and space [Carn et al., 2016]. The operation is, however, complicated by the large spread of H_2/SO_2 and H_2S/SO_2 ratios in volcanic gas emissions (Figure 8a–d), which has traditionally hampered the derivation of robust global estimates [Halmer et al., 2002, Canfield et al., 2006].

The two most recent attempts to estimate the H_2 and H_2S fluxes from global subaerial volcanism are from Canfield et al. [2006] and Stolper et al. [2021] (Table 1).

Canfield et al. [2006] compiled 21 high quality volcanic gas analyses from volcanoes in a variety of geological context, including rift-related, hot-spot related, and in subduction zones related. They found volcanic gas H_2/SO_2 and H_2S/SO_2 ratios to vary widely even in such a limited dataset, total ranges being respectively of 0.02–24 and 0.007–2.7. The median volcanic gas H_2/SO_2 and H_2S/SO_2 ratios in their subset of volcanic gas samples are 0.8 (H_2/SO_2) and 0.3 (H_2S/SO_2). Ultimately, by using most representative ratio ranges in combination with a global SO_2 flux estimate [Halmer et al., 2002] they quantified the global volcanic H_2 and H_2S fluxes at 0.2–0.7 Tg/yr and 1.4–2.0 Tg/yr, respectively (Table 1).

Stolper et al. [2021] also based their H_2 and H_2S flux estimates on major species' global budgets—they used the more updated global volcanic SO_2 and H_2O flux inventories of Fischer et al. [2019]. However, they adopted a different methodology for deriving best-estimates for H_2/SO_2 and H_2S/SO_2 ratios in "globally averaged volcanic gas emissions". Instead of averaging results from measured H_2/SO_2 and H_2S/SO_2 ratios in volcanic gas samples, they relied on thermodynamically derived H_2/SO_2 and H_2S/SO_2 ratios, calculated (from relations similar to Equations (3) and (4) presented above) at temperature, pressure and redox (fO_2) conditions of the source silicate melt. For example, they quantified the global volcanic H_2 flux at 0.07–0.44 Tg/yr (Table 1) by combining the global volcanic H_2O flux of Fischer et al. [2019] with the thermodynamically derived (Equation (3)) H_2/H_2O ratios at equilibrium with melt,

Table 1. Global volcanic H_2S and H_2 fluxes (in Tg/yr) revisited

		Mean	SD	Mean	SD	50%	25%	75%	50%	25%	75%	50%	25%	75%	50%	25%	75%
		SO_2 flux		CO_2 flux		H_2S/SO_2			H_2S flux			H_2/SO_2			H_2 flux		
S_{vge}	Magmatic	**24.9**	2.3	**36**	2.4	0.1	0.06	0.6	**1.3**	0.8	8.3	0.3	0.1	1.3	**0.23**	0.06	1.0
		SO_2 flux		CO_2 flux		H_2S/CO_2			H_2S flux			H_2/CO_2			H_2 flux		
W_{vge}	Magmatic	-	-	**11.6**	3.9	0.008	0.006	0.043	**0.08**	0.05	0.4	0.002	0.0005	0.012	**0.0012**	0.0002	0.0062
W_{vge}	Hydrothermal	-	-	**3.7**	1.2	0.008	0.006	0.043	**0.02**	0.02	0.12	0.002	0.0005	0.012	**0.0004**	0.0001	0.0020
		SO_2 flux		CO_2 flux					H_2S flux						H_2 flux		
Total	This study ($S_{vge} + W_{vge}$)	**24.9**	2.3	**51.3**	7.5				**1.4**	0.9	8.8				**0.23**	0.06	1.0
Total	Canfield et al. [2006]									**1.4–2**						**0.2–0.7**	
	Stolper et al. [2021]									**0.05–4**						**0.07–0.44**	

These are obtained by multiplying the global volcanic SO_2 and CO_2 fluxes of Fischer et al. [2019] by the median (molar) gas ratios in our catalogue (Supplementary Tables 1 and 2). See text. Uncertainty is quantified using 25 and 75 percentiles. We distinguish three volcano categories (S_{vge}, magmatic W_{vge} and hydrothermal W_{vge}) as in Fischer and Aiuppa [2020]. Total fluxes are calculated by summing together the three flux contributions. Previous flux inventories by Canfield et al. [2006] and Stolper et al. [2021] are shown for comparison.

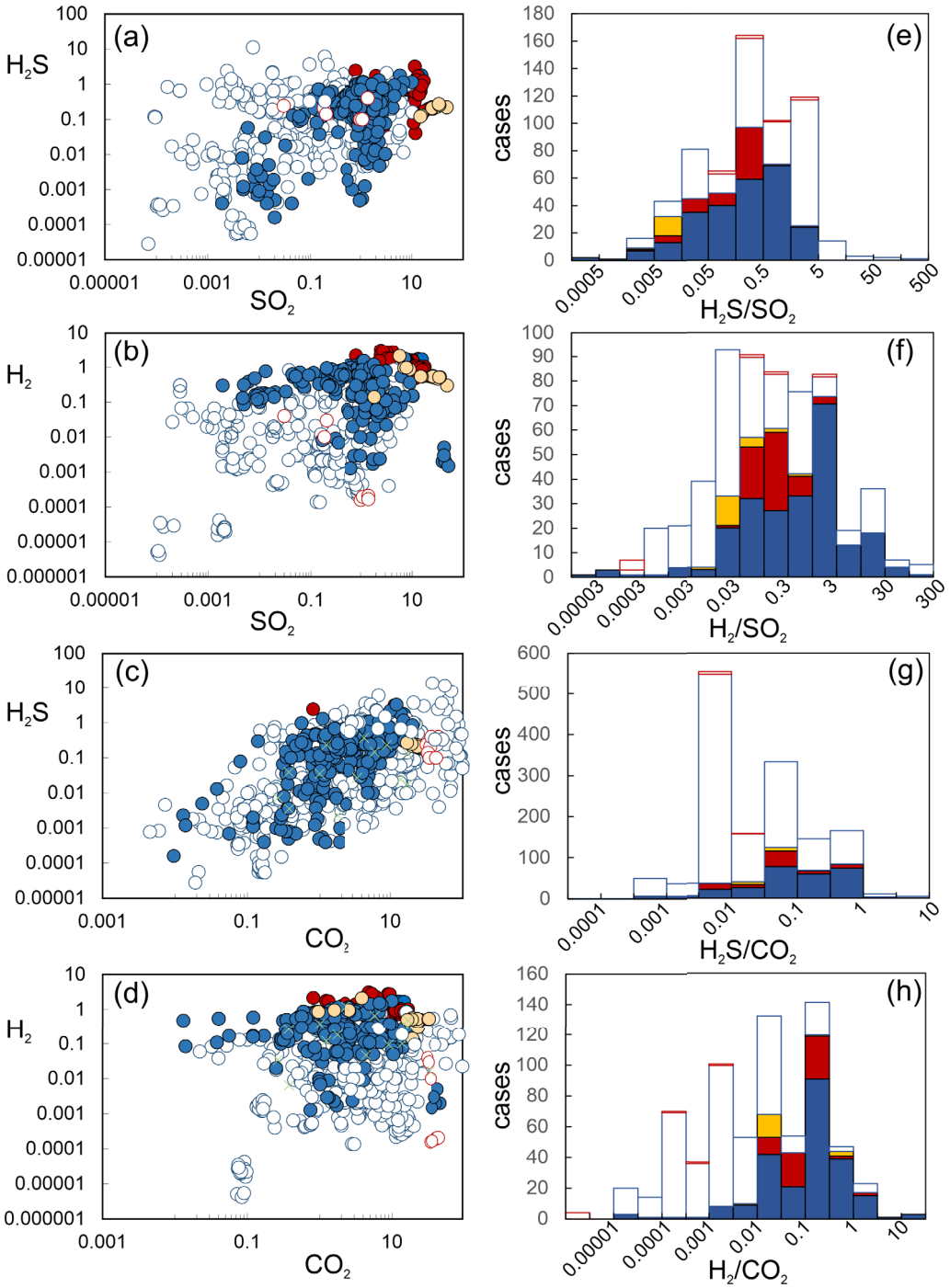

Figure 8. (a–d) Scatter plots of H_2S and H_2 concentrations (data from Supplementary Tables 1 and 2) versus major species' concentrations (either SO_2 or CO_2). All concentrations in mol%. (e–h) Frequency distribution diagrams of volatile (molar) ratios used for flux calculations. See text, symbols as in Figure 2 except green crossed [hydrothermal steam samples from Chiodini and Marini, 1998].

using T, P, fO_2 values relevant to modern subaerial magmas. Likewise, their global volcanic H_2S flux range of 0.05–4 Tg/yr was inferred from the global SO_2 inventory of Fischer et al. [2019] and the thermodynamically estimated Equation (4) equilibrium (at melt T, P, fO_2) H_2S/SO_2 ratios (Table 1). It is necessary to remember that Stolper et al. [2021] implicitly assume that surface volcanic gas emissions are controlled (buffered) by heterogenous equilibrium with the coexisting silicate melt. However, this assumption, as previously discussed (cf. Section 4.3), likely holds only for the very few cases of gases emitted at magmatic temperature, but not for the many, lower temperature gas emissions seen at the vast majority of the active volcanoes worldwide (see Figures 3, 4, 6). For example, the range of estimated equilibrium H_2/H_2O ratios of Stolper et al. [2021] is 0.01 to 0.024, and therefore captures only the upper class (the "magmatic" range) of measured H_2/H_2O ratios in volcanic gases (Figures 3a and 5); the majority of the surface-emitted volcanic gases will be far more H_2-poor because of re-equilibration during homogenous (closed-system) gas cooling (cf. Section 4.3). As magmatic gas H_2S/SO_2 are overall preserved during gas cooling (Figures 3b, 5), their estimated range (0.000012–0.28) is representative of the measured gas composition range (Figure 8b).

We here attempt at a refined H_2 and H_2S volcanic flux inventory (Table 1) by using our more complete volcanic gas catalogue (Supplementary Tables 1 and 2).

Our calculations stand on the approach developed in the most recent volcanic gas flux quantification efforts [Fischer et al., 2019, Fischer and Aiuppa, 2020], in which three categories of subaerial volcanoes are distinguished and separately treated (Table 1). A first category of Volcanic Gas Emitters (S_{vge}) includes the strongly degassing volcanoes whose SO_2 emissions can systematically be detected by satellites [e.g., Carn et al., 2017, Fischer et al., 2019]. These volcanoes typically release high-temperature, SO_2-rich gases, often from open-vent persistently degassing vents, and are believed to dominate the volcanic SO_2 and CO_2 flux inventories [e.g., Aiuppa et al., 2017, 2019, Carn et al., 2017, Fischer et al., 2019, Werner et al., 2019, Fischer and Aiuppa, 2020]. Our high-temperature (T > 600 °C; Supplementary Table 1), S_T-rich (Figure 1) magmatic gases are inherently the most representative of such emission category. These have median H_2S/SO_2 (Figure 8a–e) and H_2/SO_2 (Figure 8b–f) ratios of respectively 0.1 and 0.3 (25%–75% percentiles: 0.06–0.6 and 0.1–1.3, respectively; Table 1). From these, and scaling to the global volcanic flux SO_2 of Fischer et al. [2019] (24.9 Tg/yr), we infer the S_{vge} contribution to the global (subaerial) volcanic H_2 and H_2S flux at 1.3 Tg/yr (confidence interval, 0.8–8.3) and 0.23 Tg/yr (confidence interval, 0.06–1). The other two categories correspond to the Weak Gas Emitters (W_{vge}) [Fischer et al., 2019, Fischer and Aiuppa, 2020] that include both (a) recently active (but now dormant) volcanoes whose SO_2 emissions are too small to be resolved from space (the "magmatic" W_{vge}), or (b) quiescent volcanoes in hydrothermal stage of activity (the "hydrothermal" W_{vge}) that do not release SO_2 at all, and in which sulphur is essentially released in H_2S form. For W_{vge}, we therefore cannot rely on a SO_2 flux proxy. Rather, we use the CO_2 flux estimates of Fischer et al. [2019], in combination with H_2S/CO_2 (Figure 8c–g) and H_2/CO_2 (Figure 8d–h) ratios. Our mixed (magmatic–hydrothermal), lower temperature ($T \leq 600$ °C; Supplementary Table 2) volcanic gas population exactly corresponds to the category of "magmatic" W_{vge}, and exhibits H_2S/CO_2 and H_2/CO_2 ratios of 0.008 (0.006–0.043) and 0.002 (0.0005–0.012) (Table 1). Hydrothermal W_{vge} are not explicitly covered by our review, but their compositions [see data from Chiodini and Marini, 1998] overlap with the magmatic" W_{vge} compositional range (Figures 8g and h), so we can use the composition of the latter. In summary, therefore, we infer that W_{vge} contribute ~0.1 Tg H_2S and ~0.0016 Tg H_2 yearly. It is important to stress that the population of W_{vge} spans orders of magnitude in terms of H_2S/CO_2 and H_2/CO_2 (Figures 8c–d and g–h) ratios, so our flux estimates for this specific category are very poorly constrained. However, this has limited impact on our estimated total fluxes of H_2S (1.4 Tg/yr; 0.9–8.8) and H_2 (0.23 Tg/yr; 0.06–1) fluxes, which are by far dominated by S_{vge}. We conclude that, while thus W_{vge} are important volcanic CO_2 sources [Table 1; Fischer et al., 2019, Fischer and Aiuppa, 2020], their contribution to global volcanic subaerial fluxes of reduced, hydrogenated compounds is irrelevant. This reflects the H_2-poor signature of low temperature gas emissions (Figures 2, 3, 5, 8)—caused by gas oxidation during cooling (Figure 6) (cf. Section 4.3)—and the removal of water-soluble sulphur during magmatic

gas interactions with liquid-dominated hydrothermal systems [e.g., Aiuppa et al., 2017], which determines the prevailing low H_2S/CO_2 compositions (Figures 1, 8g). Our estimated total volcanic H_2S and H_2 fluxes are at the lower range of the estimates of Canfield et al. [2006], and at the very middle of the flux range of Stolper et al. [2021] (Table 1).

Our results indicate that global volcanism contributes little (~1%; range 0.3–4.3%) to the cumulative (global) geogenic H_2 flux [~23 Tg/yr; Zgonnik, 2020]. For comparison, anthropogenic H_2 emissions [~11 Tg/yr; Ehhalt and Rohrer, 2009] are 1 to 2 orders of magnitude higher than volcanic emissions. In contrast, our best-estimate for the volcanic H_2S flux (1.4 Tg/yr) implies volcanoes do make up a non-trivial (~18%) fraction of the global natural H_2S flux [~7.7 Tg/yr; Watts, 2000]. Volcanic degassing contributes nearly 3 times less H_2S than today anthropogenic emissions [3.3 Tg/yr; Watts, 2000].

5. Summary and conclusions

We have reviewed our present understanding of the processes that govern the abundance of reduced hydrogenated compounds in volcanic gases. Our review shows that the apparent oxygen fugacities of high-temperature volcanic gases range from ΔFMQ −1 to 0 (for non-arc volcanoes) to ΔFMQ 0 to +2 (for arc volcanoes), and are therefore comparable to the redox conditions of the source silicate melts. A variety of processes can alter gas composition and redox state (H_2/H_2O and H_2S/SO_2 ratios) as the gases expand within the melt and cool, and/or after they separate from magma on their route to the surface. Data in our catalogue, when interpreted in the context of existing models of homogeneous (gas) or heterogeneous (gas–mineral) reactions, suggest that in many cases the fast-reacting H_2/H_2O couple rapidly re-equilibrates during cooling (e.g., in low temperature gas environments) in a gas-buffered system which redox is controlled by coexisting H_2S and SO_2 (which H_2S/SO_2 ratio is ultimately conserved at ~0.1 on average). This gas-phase (closed-system) re-equilibration upon cooling causes the gas to become more oxidised than the original (source) magma [Oppenheimer et al., 2018, Moussallam et al., 2019b]. Conversion of magmatic SO_2 to hydrothermal H_2S (and precipitation of sulphates/sulphides) is instead favoured by slower transit of the gas through the host rocks, causing more prolonged gas–water–rock interactions to occur. This condition [Henley and Fischer, 2021] certainly prevails in more mature, liquid-dominated, and stable (less magma fed) hydrothermal systems [Chiodini and Marini, 1998]. Our volcanic gas dataset, combined with recently published global volcanic SO_2 and CO_2 budgets, implies total H_2S and H_2 fluxes from global subaerial volcanism of 1.4 Tg/yr (range, 0.9–8.8 Tg/yr) and 0.23 Tg/yr (range, 0.06–1 Tg/yr), respectively.

Declaration of interests

The authors do not work for, advise, own shares in, or receive funds from any organization that could benefit from this article, and have declared no affiliations other than their research organizations.

Acknowledgements

This research received financial support from the Ministero dell'Università e Ricerca (Italy, Grant n. 2017LMNLAW), from the Dipartimento della Protezione Civile and the INGV (under grant "Sviluppo del sistema unico (INGV-Università) di monitoraggio vulcanico e rilevamento precoce dei maremoti e delle esplosioni parossistiche di Stromboli"), and from the PNRR PE Project "Return". This work was initially inspired by participation of AA to the International School "Understanding Oxygen fugacity in Geoscience" 5–9 September 2022, Trieste, Italy (https://fo2school.units.it/), and the organisers of the school (Luca Ziberna and Vincenzo Stagno especially) are warmly thanked.

Supplementary data

Supporting information for this article is available on the journal's website under https://doi.org/10.5802/crgeos.235 or from the author.

References

Aiuppa, A. (2015). Volcanic-gas monitoring. In Schmidt, A., Fristad, K. E., and Elkins-Tanton, L. T., editors, *Volcanism and Global Environmental Change*, pages 81–96. Cambridge University Press, Cambridge, UK.

Aiuppa, A., Casetta, F., Coltorti, M., Stagno, V., and Tamburello, G. (2021). Carbon concentration increases with depth of melting in Earth's upper mantle. *Nat. Geosci.*, 14, 697–703.

Aiuppa, A., Fischer, T. P., Plank, T., and Bani, P. (2019). CO_2 flux emissions from the Earth's most actively degassing volcanoes, 2005–2015. *Sci. Rep.*, 9, article no. 5442.

Aiuppa, A., Fischer, T. P., Plank, T., Robidoux, P., and Di Napoli, R. (2017). Along-arc, inter-arc and arc-to-arc variations in volcanic gas CO_2/ST ratios reveal dual source of carbon in arc volcanism. *Earth-Sci. Rev.*, 168, 24–47.

Aiuppa, A., Franco, A., Glasow, R. V., Allen, A. G., D'Alessandro, W., and Mather, T. A. (2007). The tropospheric processing of acidic gases and hydrogen sulphide in volcanic gas plumes as inferred from field and model investigations. *Atmos. Chem. Phys.*, 7, 1441–1450.

Aiuppa, A., Inguaggiato, S., McGonigle, A. J. S., O'Dwyer, M., Oppenheimer, C., Padgett, M. J., Rouwet, D., and Valenza, M. (2005). H2S fluxes from Mt. Etna, Stromboli, and Vulcano (Italy) and implications for the sulfur budget at volcanoes. *Geochim. Cosmochim. Acta*, 69, 1861–1871.

Aiuppa, A., Shinohara, H., Tamburello, G., Giudice, G., Liuzzo, M., and Moretti, R. (2011). Hydrogen in the gas plume of an open-vent volcano, Mount Etna, Italy. *J. Geophys. Res.*, 116, B10204.

Aiuppa, A., Tamburello, G., Di Napoli, R., Cardellini, C., Chiodini, G., Giudice, G., Grassa, F., and Pedone, M. (2013). First observations of the fumarolic gas output from a restless caldera: Implications for the current period of unrest (2005–2013) at Campi Flegrei. *Geochem. Geophys. Geosyst.*, 14(10), 4153–4169.

Allard, P., Aiuppa, A., Beatuducel, F., Gaudin, D., Di Napoli, R., Calabrese, S., Parello, F., Crispi, O., Hammouya, G., and Tamburello, G. (2014). Steam and gas emission rate from La Soufriere volcano, Guadeloupe (Lesser Antilles): Implications for the magmatic supply during degassing unrest. *Chem. Geol.*, 384, 76–93.

Arellano, S., Galle, B., Apaza, F., Avard, G., Barrington, C., Bobrowski, N., Bucarey, C., Burbano, V., Burton, M., Chacón, Z., Chigna, G., Clarito, C. J., Conde, V., Costa, F., De Moor, M., Delgado-Granados, H., Di Muro, A., Fernandez, D., Garzón, G., Gunawan, H., Haerani, N., Hansteen, T. H., Hidalgo, S., Inguaggiato, S., Johansson, M., Kern, C., Kihlman, M., Kowalski, P., Masias, P., Montalvo, F., Möller, J., Platt, U., Rivera, C., Saballos, A., Salerno, G., Taisne, B., Vásconez, F., Velásquez, G., Vita, F., and Yalire, M. (2021). Synoptic analysis of a decade of daily measurements of SO_2 emission in the troposphere from volcanoes of the global ground-based network for observation of volcanic and atmospheric change. *Earth Syst. Sci. Data*, 13, 1167–1188.

Brounce, M., Stolper, E., and Eiler, J. (2017). Redox variations in Mauna Kea lavas, the oxygen fugacity of the Hawaiian plume, and the role of volcanic gases in Earth's oxygenation. *Proc. Natl. Acad. Sci. USA*, 114, 8997–9002.

Burgisser, A. and Scaillet, B. (2007). Redox evolution of a degassing magma rising to the surface. *Nature*, 445, 194–197.

Canfield, D. E., Rosing, M. T., and Bjerrum, C. (2006). Early anaerobic metabolisms. *Philos. Trans. R. Soc. Lond. B*, 361, 1819–1834. Discussion 1835–1836.

Carn, S. A., Clarisse, L., and Prata, A. J. (2016). Multi-decadal satellite measurements of global volcanic degassing. *J. Volcanol. Geotherm. Res.*, 311, 99–134.

Carn, S. A., Fioletov, V. E., McLinden, C. A., Li, C., and Krotkov, N. A. (2017). A decade of global volcanic SO_2 emissions measured from space. *Sci. Rep.*, 7, article no. 44095.

Chase, M. W. and National Institute of Standards and Technology (U.S.) (1998). *NIST-JANAF Thermochemical Tables*. American Chemical Society; American Institute of Physics for the National Institute of Standards and Technology, Washington, DC; Woodbury, NY.

Chiodini, G., Cioni, R., and Marini, L. (1993). Reactions governing the chemistry of crater fumaroles from Vulcano Island, Italy, and implications for volcanic surveillance. *Appl. Geochem.*, 8, 357–371.

Chiodini, G. and Marini, L. (1998). Hydrothermal gas equilibria: the H_2O-H_2-CO_2-CO-CH_4 system. *Geochim. Cosmochim. Acta*, 62, 2673–2687.

Cicconi, M. R., Moretti, R., and Neuville, D. R. (2020). Earth's electrodes. *Elements*, 16, 157–160.

Cottrell, E., Birner, S., Brounce, M., Davis, F., Waters, L., and Kelley, K. (2022). Oxygen fugacity across tectonic settings. In Moretti, R. and Neuville, D. R., editors, *Magma Redox Geochemistry*, Geophysical Monograph 266. American Geophysical Union, John Wiley & Sons.

D'Amore, F. and Panichi, C. (1980). Evaluation of deep temperatures of hydrothermal systems by a new gas geothermometer. *Geochim. Cosmochim. Acta*, 44, 549–556.

de Moor, J. M., Stix, J., Avard, G., Muller, C., Corrales, E., Diaz, J. A., Alan, A., Brenes, J., Pacheco, J., Aiuppa, A., and Fischer, T. P. (2019). Insights on hydrothermal–magmatic interactions and eruptive processes at Poás Volcano (Costa Rica) from high-frequency gas monitoring and drone measurements. *Geophys. Res. Lett.*, 46, 1293–1302.

Ehhalt, D. H. and Rohrer, F. (2009). The tropospheric cycle of H_2: a critical review. *Tellus B Chem. Phys. Meteorol.*, 61, 500–535.

Ellis, A. J. (1957). Chemical equilibrium in magmatic gases. *Am. J. Sci.*, 255, 416–431.

Eugster, H. P. (1977). Compositions and thermodynamics of metamorphic solutions. In *Thermodynamics in Geology: Proceedings of the NATO Advanced Study Institute Held in Oxford, England, September 17–27, 1976*, pages 183–202. D. Reidel Publishing Company, Dordrecht, Holland/Boston, USA.

Evans, K. A. (2012). The redox budget of subduction zones. *Earth-Sci. Rev.*, 113, 11–32.

Fischer, T. P. (2008). Fluxes of volatiles (H_2O, CO_2, N_2, Cl, F) from arc volcanoes. *Geochem. J.*, 42, 21–38.

Fischer, T. P. and Aiuppa, A. (2020). AGU Centennial Grand Challenge: Volcanoes and deep carbon global CO_2 emissions from subaerial volcanism—Recent progress and future challenges. *Geochem. Geophys. Geosyst.*, 21, article no. e2019GC008690.

Fischer, T. P., Arellano, S., Carn, S., Aiuppa, A., Galle, B., Allard, P., Lopez, T., Shinohara, H., Kelly, P., Werner, C., Cardellini, C., and Chiodini, G. (2019). The emissions of CO_2 and other volatiles from the world's subaerial volcanoes. *Sci. Rep.*, 9, article no. 18716.

Fischer, T. P. and Chiodini, G. (2015). Chapter 45 – Volcanic, magmatic and hydrothermal gases. In Sigurdsson, H., editor, *The Encyclopedia of Volcanoes*, pages 779–797. Academic Press, Amsterdam, 2nd edition.

Frost, B. R. (1991). Introduction to oxygen fugacity and its petrologic importance. *Rev. Mineral. Geochem.*, 25, 1–9.

Frost, D. J. and McCammon, C. A. (2008). The redox state of Earth's mantle. *Annu. Rev. Earth Planet. Sci.*, 36, 389–420.

Gaillard, F. and Scaillet, B. (2014). A theoretical framework for volcanic degassing chemistry in a comparative planetology perspective and implications for planetary atmospheres. *Earth Planet. Sci. Lett.*, 403, 307–316.

Gaillard, F., Scaillet, B., and Arndt, N. T. (2011). Atmospheric oxygenation caused by a change in volcanic degassing pressure. *Nature*, 478, 229–232.

Gaillard, F., Scaillet, B., Pichavant, M., and Iacono-Marziano, G. (2015). The redox geodynamics linking basalts and their mantle sources through space and time. *Chem. Geol.*, 418, 217–233.

Gerlach, T. M. (1979). Evaluation and restoration of the 1970 volcanic gas analyses from Mount Etna, Sicily. *J. Volcanol. Geotherm. Res.*, 6, 165–178.

Gerlach, T. M. (1980). Evaluation of volcanic gas analyses from Kilauea volcano. *J. Volcanol. Geotherm. Res.*, 7, 295–317.

Gerlach, T. M. (1982). Interpretation of volcanic gas data from tholeiitic and Alkaline Mafic Lavas. *Bull. Volcanol.*, 45, 235–244.

Gerlach, T. M. (1993a). Oxygen buffering of Kilauea volcanic gases and the oxygen fugacity of Kilauea basalt. *Geochim. Cosmochim. Acta*, 57(4), 795–814.

Gerlach, T. M. (1993b). Thermodynamic evaluation and restoration of volcanic gas analysis: An example based on modern collection and analytical methods. *Geochem. J.*, 27, 305–322.

Gerlach, T. M. and Nordlie, B. E. (1975). The C-O-H-S gaseous system; Part II, Temperature, atomic composition, and molecular equilibria in volcanic gases. *Am. J. Sci.*, 275, 377–394.

Giggenbach, W. F. (1980). Geothermal gas equilibria. *Geochim. Cosmochim. Acta*, 44, 2021–2032.

Giggenbach, W. F. (1987). Redox processes governing the chemistry of fumarolic gas discharges from White Island, New Zealand. *Appl. Geochem.*, 2, 143–161.

Giggenbach, W. F. (1996). Chemical composition of volcanic gases. In Scarpa, R. and Tilling, R. I., editors, *Monitoring and Mitigation of Volcano Hazards*, pages 221–256. Springer Verlag, Berlin.

Giggenbach, W. F. (1997). The origin and evolution of fluids in magmatic-hydrothermal systems. In Barnes, H. L., editor, *Geochemistry of Hydrothermal Ore Deposits*, pages 737–796. John Wiley & Sons Inc, New York.

Gilat, A. L. and Vol, A. (2012). Degassing of primordial hydrogen and helium as the major energy source

for internal terrestrial processes. *Geosci. Front.*, 3, 911–921.

Halmer, M. M., Schmincke, H.-U., and Graf, H.-F. (2002). The annual volcanic gas input into the atmosphere, in particular into the stratosphere: a global data set for the past 100 years. *J. Volcanol. Geotherm. Res.*, 115, 511–528.

Helz, R. T., Cottrell, E., Brounce, M. N., and Kelley, K. A. (2017). Olivine-melt relationships and syneruptive redox variations in the 1959 eruption of Kīlauea Volcano as revealed by XANES. *J. Volcanol. Geotherm. Res.*, 333–334, 1–14.

Henley, R. W. and Berger, B. R. (2011). Magmatic-vapor expansion and the formation of high-sulfidation gold deposits: Chemical controls on alteration and mineralization. *Ore Geol. Rev.*, 39, 63–74.

Henley, R. W. and Fischer, T. P. (2021). Sulfur sequestration and redox equilibria in volcanic gases. *J. Volcanol. Geotherm. Res.*, 414, article no. 107181.

Henley, R. W., King, P. L., Wykes, J. L., Renggli, C. J., Brink, F. J., Clark, D. A., and Troitzsch, U. (2015). Porphyry copper deposit formation by sub-volcanic sulphur dioxide flux and chemisorption. *Nat. Geosci.*, 8, 210–215.

Henley, R. W. and Seward, T. M. (2018). Gas–solid reactions in arc volcanoes: Ancient and modern. *Rev. Mineral. Geochem.*, 84, 309–349.

Holland, H. D. (2002). Volcanic gases, black smokers, and the great oxidation event. *Geochim. Cosmochim. Acta*, 66, 3811–3826.

Kasting, J. F., Eggler, D. H., and Raeburn, S. P. (1993). Mantle redox evolution and the oxidation state of the Archean atmosphere. *J. Geol.*, 101, 245–257.

Kern, C., Aiuppa, A., and de Moor, J. M. (2022). A golden era for volcanic gas geochemistry? *Bull. Volcanol.*, 84, article no. 43.

Le Guern, F., Carbonnelle, J., and Tazieff, H. (1979). Erta'ale lava lake: heat and gas transfer to the atmosphere. *J. Volcanol. Geotherm. Res.*, 6, 27–48.

Martin, R. S., Mather, T. A., and Pyle, D. M. (2006). High-temperature mixtures of magmatic and atmospheric gases. *Geochem. Geophys. Geosyst.*, 7(4), 1–14.

Matsuo, S. (1962). Establishment of chemical equilibrium in the volcanic gas obtained from the lava lake of Kilauea, Hawaii. *Bull. Volcanol.*, 24, 59–71.

Moretti, R. (2021). Ionic syntax and equilibrium approach to redox exchanges in melts: basic concepts and the case of iron and sulfur in degassing magmas. In *Magma Redox Geochemistry*, AGU Gophysical Monograph 266, pages 115–138. John Wiley & Sons, New York.

Moretti, R., Komorowski, J.-C., Ucciani, G., Moune, S., Jessop, D., de Chabalier, J.-B., Beauducel, F., Bonifacie, M., Burtin, A., Vallée, M., Deroussi, S., Robert, V., Gibert, D., Didier, T., Kitou, T., Feuillet, N., Allard, P., Tamburello, G., Shreve, T., Saurel, J.-M., Lemarchand, A., Rosas-Carbajal, M., Agrinier, P., Le Friant, A., and Chaussidon, M. (2020). The 2018 unrest phase at La Soufrière of Guadeloupe (French West Indies) andesitic volcano: Scrutiny of a failed but prodromal phreatic eruption. *J. Volcanol. Geotherm. Res.*, 393, article no. 106769.

Moretti, R. and Neuville, D. R. (2021). *Magma Redox Geochemistry*. Geophysical Monograph 266, AGU Geophysical Monograph Series. John Wiley & Sons, Hoboken, NJ, USA.

Moretti, R. and Stefánsson, A. (2020). Volcanic and geothermal redox engines. *Elements*, 16, 179–184.

Moune, S., Moretti, R., Burtin, A., Jessop, D. E., Didier, T., Robert, V., Bonifacie, M., Tamburello, G., Komorowski, J.-C., Allard, P., and Buscetti, M. (2022). Gas monitoring of volcanic-hydrothermal plumes in a tropical environment: The case of La Soufrière de Guadeloupe Unrest Volcano (Lesser Antilles). *Front. Earth Sci.*, 10, article no. 795760.

Moussallam, Y., Edmonds, M., Scaillet, B., Peters, N., Gennaro, E., Sides, I., and Oppenheimer, C. (2016). The impact of degassing on the oxidation state of basaltic magmas: A case study of Kīlauea volcano. *Earth Planet. Sci. Lett.*, 450, 317–325.

Moussallam, Y., Longpré, M.-A., McCammon, C., Gomez-Ulla, A., Rose-Koga, E. F., Scaillet, B., Peters, N., Gennaro, E., Paris, R., and Oppenheimer, C. (2019a). Mantle plumes are oxidised. *Earth Planet. Sci. Lett.*, 527, article no. 115798.

Moussallam, Y., Oppenheimer, C., Aiuppa, A., Giudice, G., Moussallam, M., and Kyle, P. (2012). Hydrogen emissions from Erebus volcano, Antarctica. *Bull. Volcanol.*, 74, 2109–2120.

Moussallam, Y., Oppenheimer, C., and Scaillet, B. (2019b). On the relationship between oxidation state and temperature of volcanic gas emissions. *Earth Planet. Sci. Lett.*, 520, 260–267.

Moussallam, Y., Oppenheimer, C., and Scaillet, B. (2022). A novel approach to volcano surveillance using gas geochemistry. *C. R. Géosci.*, 356, 1–14.

Moussallam, Y., Oppenheimer, C., Scaillet, B., Gaillard, F., Kyle, P., Peters, N., Hartley, M., Berlo, K., and Donovan, A. (2014a). Tracking the changing oxidation state of Erebus magmas, from mantle to surface, driven by magma ascent and degassing. *Earth Planet. Sci. Lett.*, 393, 200–209.

Moussallam, Y., Peters, N., Ramírez, C., Oppenheimer, C., Aiuppa, A., and Giudice, G. (2014b). Characterisation of the magmatic signature in gas emissions from Turrialba Volcano, Costa Rica. *Solid Earth*, 5, 1341–1350.

Ohba, T., Hirabayashi, J., and Yoshida, M. (1994). Equilibrium temperature and redox state of volcanic gas at Unzen volcano, Japan. *J. Volcanol. Geotherm. Res.*, 60, 263–272.

Oppenheimer, C., Scaillet, B., Woods, A., Sutton, A. J., Elias, T., and Moussallam, Y. (2018). Influence of eruptive style on volcanic gas emission chemistry and temperature. *Nat. Geosci.*, 11, 678–681.

Roberts, T., Dayma, G., and Oppenheimer, C. (2019). Reaction rates control high-temperature chemistry of volcanic gases in air. *Front. Earth Sci.*, 7, article no. 154.

Seinfeld, J. H. and Pandis, S. N. (2016). *Atmospheric Chemistry and Physics: From Air Pollution to Climate Change*. John Wiley & Sons, New York, USA.

Shinohara, H. (2005). A new technique to estimate volcanic gas composition: plume measurements with a portable multi-sensor system. *J. Volcanol. Geotherm. Res.*, 143, 319–333.

Shinohara, H., Giggenbach, W. F., Kazahaya, K., and Hedenquist, J. W. (1993). Geochemistry of volcanic gases and hot springs of Satsuma-Iwojima, Japan: following Matsuo. *Geochem. J.*, 27, 271–285.

Shinohara, H., Matsushima, N., Kazahaya, K., and Ohwada, M. (2011). Magma-hydrothermal system interaction inferred from volcanic gas measurements obtained during 2003–2008 at Meakandake volcano, Hokkaido, Japan. *Bull. Volcanol.*, 73, 409–421.

Shinohara, H., Ohminato, T., Takeo, M., Tsuji, H., and Kazahaya, R. (2015). Monitoring of volcanic gas composition at Asama volcano, Japan, during 2004–2014. *J. Volcanol. Geotherm. Res.*, 303, 199–208.

Shinohara, H., Yokoo, A., and Kazahaya, R. (2018). Variation of volcanic gas composition during the eruptive period in 2014–2015 at Nakadake crater, Aso volcano, Japan. *Earth Planet. Space*, 70, 1–21.

Stagno, V., Ojwang, D. O., McCammon, C. A., and Frost, D. J. (2013). The oxidation state of the mantle and the extraction of carbon from Earth/'s interior. *Nature*, 493, 84–88.

Stix, J. and de Moor, J. M. (2018). Understanding and forecasting phreatic eruptions driven by magmatic degassing. *Earth Planet. Space*, 70, article no. 83.

Stolper, D. A., Higgins, J. A., and Derry, L. A. (2021). The role of the solid earth in regulating atmospheric O_2 levels. *Am. J. Sci.*, 321, 1381–1444.

Surono, Jousset, P., Pallister, J., Boichu, M., Buongiorno, M. F., Budisantoso, A., Costa, F., Andreastuti, S., Prata, F., Schneider, D., Clarisse, L., Humaida, H., Sumarti, S., Bignami, C., Griswold, J., Carn, S., Oppenheimer, C., and Lavigne, F. (2012). The 2010 explosive eruption of Java's Merapi volcano—A '100-year' event. *J. Volcanol. Geotherm. Res.*, 241–242, 121–135.

Symonds, R. B., Gerlach, T. M., and Reed, M. H. (2001). Magmatic gas scrubbing: implications for volcano monitoring. *J. Volcanol. Geotherm. Res.*, 108, 303–341.

Symonds, R. B., Rose, W. I., Bluth, G. J. S., and Gerlach, T. M. (1994). Volcanic-gas studies; methods, results, and applications. *Rev. Mineral. Geochem.*, 30, 1–66.

Tamburello, G., Moune, S., Allard, P., Venugopal, S., Robert, V., Rosas-Carbajal, M., Deroussi, S., Kitou, G.-T., Didier, T., Komorowski, J.-C., Beauducel, F., De Chabalier, J.-B., Le Marchand, A., Le Friant, A., Bonifacie, M., Dessert, C., and Moretti, R. (2019). Spatio-temporal relationships between fumarolic activity, hydrothermal fluid circulation and geophysical signals at an arc volcano in degassing unrest: La soufrière of guadeloupe (French West Indies). *Geosciences (Switzerland)*, 9(11), article no. 480.

Taran, Y. and Zelenski, M. (2015). In *Systematics of Water Isotopic Composition and Chlorine Content in Arc-volcanic Gases*, Geological Society, London, Special Publications 410, pages 237–262. Geological Society of London.

Warneck, P. (1988). *Chemistry of the Natural Atmosphere*, volume 41 of *International Geophysics Series*. Academic Press, San Diego, CA.

Watts, S. F. (2000). The mass budgets of carbonyl sulfide, dimethyl sulfide, carbon disulfide and hydrogen sulfide. *Atmos. Environ.*, 34, 761–779.

Werner, C., Fischer, T. P., Aiuppa, A., Edmonds, M., Cardellini, C., Carn, S., Chiodini, G., Cottrell, E., Burton, M., and Shinohara, H. (2019). Carbon dioxide emissions from subaerial volcanic regions. In *Deep Carbon Past to Present*. Cambridge University Press, Cambridge, UK.

Zgonnik, V. (2020). The occurrence and geoscience of natural hydrogen: A comprehensive review. *Earth-Sci. Rev.*, 203, article no. 103140.